Journal of Dentistry 139 (2023) 104761

Contents lists available at ScienceDirect

Journal of Dentistry

journal homepage: www.elsevier.com/locate/jdent

A novel post-processing strategy to improve the accuracy of complete-arch intraoral scanning for implants: an *in vitro* study

Yu Pan [a], Xuanyi Dai [a], Fang Wan [b], Chaoyang Song [c], James KH Tsoi [d], Edmond HN Pow [d,*]

[a] Department of Dentistry, Shenzhen People's Hospital (The Second Clinical Medical College, Jinan University, The First Affiliated Hospital, Southern University of Science and Technology), Shenzhen, Guangdong, China
[b] School of Design, Southern University of Science and Technology, Shenzhen, Guangdong, China
[c] Department of Mechanical and Energy Engineering, Southern University of Science and Technology, Shenzhen, Guangdong, China
[d] Faculty of Dentistry, The University of Hong Kong, 3/F, Prince Philip Dental Hospital, 34 Hospital Road, Sai Ying Pun, Hong Kong special administrative region of China

ARTICLE INFO

Keywords:
Computer-aided design
Dimensional measurement accuracy
3-D imaging
Dental implants
Edentulous

ABSTRACT

Objectives: To develop a new post-processing strategy that utilizes an auxiliary device to adjust intraoral scans and improve the accuracy of 3D models of complete-arch dental implants.
Materials and methods: An edentulous resin model with 6 dental implants was prepared. An auxiliary device, consisting of an opaque base and artificial landmarks, was fabricated and mounted onto the resin model. Twenty intraoral scans (raw scans) were taken using this setup. A new post-processing strategy was proposed to adjust the raw scans using reverse engineering software (verified group). Additionally, ten conventional gypsum casts were duplicated and digitized using a laboratory scanner. The linear and angular trueness and precision of the models were evaluated and compared. The effect of the proposed strategy on the accuracy of complete-arch intraoral scans was analyzed using one-way ANOVA.
Results: The linear trueness (29.7 μm) and precision (24.8 μm) of the verified group were significantly better than the raw scans (46.6 μm, 44.7 μm) and conventional casts (51.3 μm, 36.5 μm), particularly in cross-arch sites. However, the angular trueness (0.114°) and precision (0.085°) of the conventional casts were significantly better than both the verified models (0.298°, 0.168°) and the raw scans (0.288°, 0.202°).
Conclusions: The novel post-processing strategy is effective in enhancing the linear accuracy of complete-arch implant IO scans, especially in cross-arch sites. However, further improvement is needed to eliminate the angular deviations.
Clinical significance: Errors generated from intraoral scanning in complete edentulous arches exceed the clinical threshold. The elimination of stitching errors in the raw scans particularly in the cross-arch sites, through the proposed post-processing strategy would enhance the accuracy of complete-arch implant prostheses.

1. Introduction

Fixed implant-supported prostheses are gaining significant popularity among complete edentulous patients owing to their remarkable oral functionality and enhanced comfort, coupled with consistently favorable clinical outcomes. The advent of optical 3D scanning and CAD-CAM technology has notably simplified and expedited the digital implant workflow in comparison to the conventional methods [1]. By utilizing handheld intraoral scanners (IOS), it is now possible to directly capture precise 3D images of the oral cavity, thus eliminating the need for traditional and often uncomfortable impressions, which are generally disliked by most patients. Previous research has showcased that IOS can achieve a high level of accuracy, with trueness ranging from 6 to 45 μm, and deliver predictable long-term results in cases involving short-span tooth-supported prostheses [2]. However, it is important to note that the current accuracy of IOS remains inadequate and clinically unacceptable when it comes to complete dentate arches, where trueness has been reported to range from 70 to 155 μm. Similarly, for cases involving multiple implants in completely edentulous arches, the reported trueness ranges from 17 to 259 μm [3–6].

The occurrence of errors in intraoral complete-arch implant scanning is widely acknowledged and can be attributed to several factors. These factors include the utilization of scan bodies, inadequate presence of anatomic landmarks, and the algorithm employed for image stitching

* Corresponding author.
E-mail address: ehnpow@hku.hk (E.H. Pow).

https://doi.org/10.1016/j.jdent.2023.104761
Received 1 June 2023; Received in revised form 18 October 2023; Accepted 22 October 2023
Available online 23 October 2023

[7–9]. A wealth of research has been conducted to thoroughly investigate the accuracy of different types and materials of scan bodies, with a preference observed for long and narrow scan bodies that possess a simple design and tight manufacturing tolerance [10–12]. To address the issue of insufficient anatomic landmarks, various auxiliary devices incorporating fiducial markers for registration have been developed [13–15]. Studies have demonstrated the effectiveness of tooth-shaped landmarks in reducing cross-arch deviations by approximately 60 μm, while the implementation of an opaque base to cover the mucosa in edentulous areas may lead to a reduction of short-span deviations by approximately 20 μm [14]. Despite these notable advancements, deviations of approximately 80 μm still persist at cross-arch sites.

The scientific evidence regarding image stitching algorithms for intraoral scanners (IOS) is currently lacking. Although one study reported a stitching error ranging from 1.9 to 18.2 μm for a three-unit span [16], accurately measuring the cumulative stitching error resulting from complete-arch IOS scans, considering different alignment methods and operative details, presents a significant challenge. Complicating matters further, all IOS products currently available on the market operate as closed systems with highly automated mechanisms and non-modifiable parameters during data processing. The process of 3D reconstruction is often regarded as a "closed black-box," with limited knowledge regarding the specific algorithms and operative details [17,18]. Consequently, addressing algorithmic errors by modifying the IOS operating systems proves to be difficult due to the lack of transparency and accessibility to the underlying processes.

Is it feasible to modify the raw images after data acquisition? A study highlighted the use of a post-processing correction module within customized software to address image distortions caused by curved focal planes in confocal microscopy [19]. The findings of this study demonstrated a significant enhancement in scanning accuracy, particularly in the X- and Y-axes of the first quadrant and the Z-axis of the second quadrant. Consequently, it suggests the possibility of rectifying cumulative errors at cross-arch sites by applying post-processing techniques to the raw scans after 3D reconstruction.

In a related context, a proposed post-processing strategy based on computer-aided design (CAD) software was introduced, utilizing a previously developed auxiliary device, with the aim of improving the accuracy of complete-arch implant intraoral scanning. The objective of this particular study was to evaluate the impact of post-processing on the accuracy of complete-arch implant intraoral scanning models. The null hypothesis put forth posited that there would be no significant difference in the linear and angular trueness/precision between the post-processed scans, raw scans, and conventional gypsum casts.

2. Materials and methods

All experiments were conducted in the same laboratory under standard conditions, with a room temperature of 25±1 ℃, a humidity level of 60 %, and an air pressure of 1050 hPa.

2.1. Preparation of the master model

A resin model of edentulous maxilla was used as the master model, with six bone-level dummy implants (NobelActive, internal RP, ø4.3/10 mm, Nobel Biocare AB, Goteborg, Sweden) inserted in parallel (Fig. 1a). The implants were connected to six multi-unit abutments (MUA Plus, Nobel Biocare AB) using a torque-controlled wrench.

2.2. Conventional impressions

Six implant impression copings (Impression Coping Open Tray Multi-unit 29089, Nobel Biocare AB) were attached to the MUAs and secured with a 1.5 mm-diameter stainless steel wire and light-cured resin (Teric N-flow, Ivoclar Vivadent, Liechtenstein) (Fig. 1b). Ten pick-up abutment-level impressions were taken using polyether impression material and custom trays (Impregum Soft, 3M ESPE, USA). Six implant analogues (multi-unit abutment replica, Nobel Biocare AB) were connected to the copings, and the impressions were poured with dental stone (Dentstone KD, Sain-Gobain, France).

2.3. Data acquisition

The MUAs were initially secured with scan bodies (Zfx^{TM} intrascan/

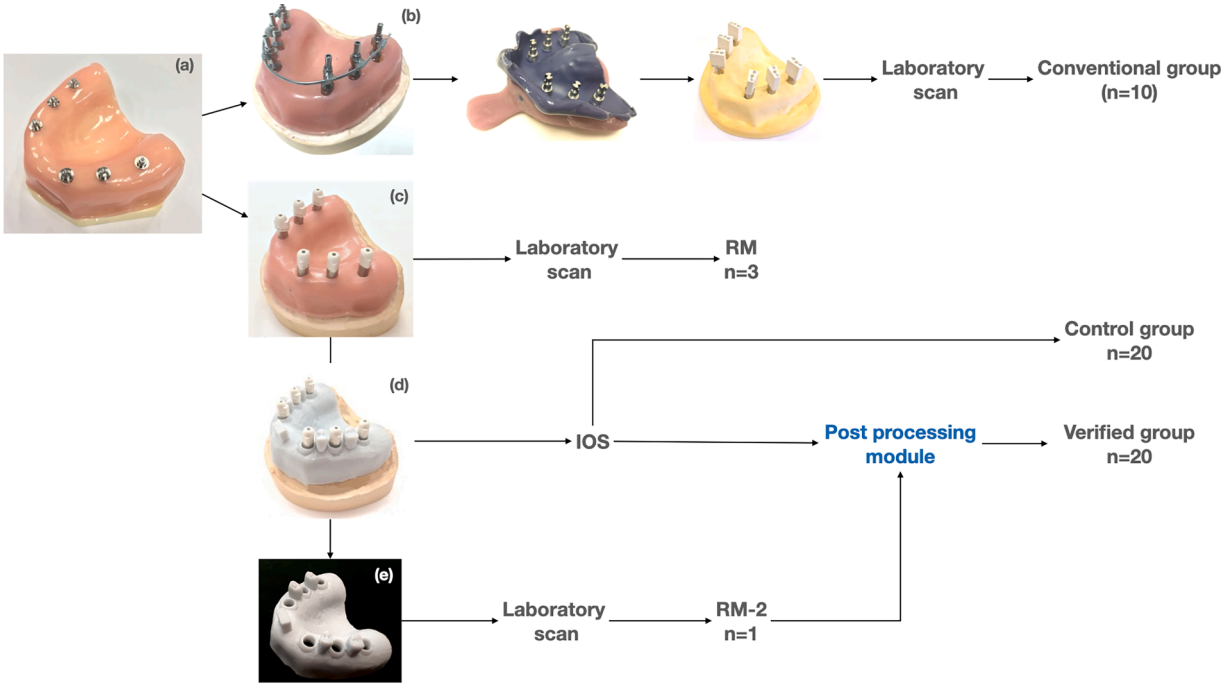

Fig. 1. Experiment outline. (a) Master model. (b) Splinted impression copings (c) Scan bodies attached. (d) Auxiliary device placed on the master model. (e) Auxiliary device alone.

evolution matchholder, Zimmer Biomet, USA) using a torque-controlled wrench. The master model was scanned three times using a high-precision structured light scanner (IScan D104i, iMetric, Courgenay, Switzerland) to serve as the reference model (RM group, $n = 3$). The same scanning process was performed on the gypsum casts (conventional group, $n = 10$). Next, a developed 3D-printed auxiliary device, consisting of an opaque base and artificial landmarks between the implants, was applied to the master model [14] (Fig. 2). The assembly was scanned using a confocal microscopy intraoral scanner (Trios 3, 3ShapeA/S, Copenhagen, Denmark), following the manufacturer's instructions (control group, $n = 20$). An additional laboratory scan was taken of the auxiliary device alone (IScan D104i), which served as a reference during post-processing (RM-2, $n = 1$). All scanning operations were performed by a single operator (Y Pan). All scan models were exported in STL format.

2.4. Post processing

All STL files were imported to reverse engineering software (Geomagic Control 2014, Geomagic, Morrisville, USA). The post-processing strategy was as follows:

1) The raw scans were segmented into six segments, consisting of four posterior and two anterior segments. Each segment included a scan body and its adjacent markers (Fig. 3). Each segment was saved as a separate STL model (test).
2) The laboratory scan of the auxiliary device (RM-2) was cropped to remove the base part, leaving only the geometric markers for registration in the subsequent alignment (the red part).
3) For each test model, the coronal two-thirds of the markers were selected as the field of interest (FOI, the red part).
4) The red part of both the test and reference models were superimposed using a two-step alignment method: three points were manually identified in the paired models for the initial matching. Then, an iterative-closest-point algorithm (ICP) was implemented to refine the alignment (sampling 5000 points, tolerance 10 μm).
5) Sequential alignments of the test models from #16 to #26 were performed (Fig. 4).
6) The aligned segments were then merged into a single 3D model.

As a result, 20 verified models were created (verified group, $n = 20$).

Fig. 2. The auxiliary device.

2.5. Evaluation of the intra-operator reliability

To ensure the reliability of subsequent measurements, the intra-operator reliability was assessed by Intra-class Correlation Coefficient (ICC). Five repeated linear and angular measurements were collected from the same original IO model, following the aforementioned protocol, by the same operator (Y. Pan). Additionally, the repeatability standard deviation of the repeated measurements was used to represent the precision of the post-processing technique.

2.6. Accuracy analysis

The RM and the three groups of models were imported into a dental software program (EXOCAD, Woburn, MA, USA), which allowed for the creation of virtual models of the MUAs based on the implant library. Geometric features, such as the bottom plane, the center-axis, and their intersection points (the Z-point), were defined on each MUA (Fig. 5). Inter-Z-point distances and angles of the center-axes between #16 and the other MUAs (16-14, 16-12, 16-22, 16-24, 16-26) were measured (Fig. 6). The reference values for these measurements were obtained from the RM group and were calculated by averaging three measurements. Accuracy was defined as the closeness between the test values and the reference values, as described by trueness and precision according to ISO-5725. Trueness was determined by calculating the mean absolute difference between the test and reference values (test-ref), while precision was represented by the standard deviation.

2.7. Statistical analysis

A pilot study was conducted to compare the linear trueness among groups ($n = 3$). The sample size was calculated using G*power (Heinrich Heine, Universität Düsseldorf, Germany) with a power of 90 % at an α-level of 0.05. ANOVA F-test was used to compare the conventional group (mean 53.0 μm), control group (mean 46.8 μm), and verified groups (35.4 μm), and a high effect size was achieved ($f = 1.028$), indicating that at least 6 scans were needed per group. To compare the cross-arch trueness, at least 16 samples were needed for the verified (mean 28.3 μm) and control group (mean 75.6 μm) with a power of 90 % at an α-level of 0.05 ($f = 1.219$).

In this study, the test variable was the post-processing of the models, and the outcome measurements were linear and angular deviations. Subgroup analyses were conducted on specific quadrants (Q1 and Q2) and implant sites (16-12, 16-14, 16-22, 16-24, 16-26). Data analysis was performed using SPSS 24.0 (IBM SPSS software; IBM Corporation, Cary, NC, USA). The normality assumption and equivalence assumptions for variance of the grouped data were assessed using the Kolmogorov-Smirnov test and Levene's test, respectively. One-way ANOVA was used to evaluate the effect of post-processing on linear and angular trueness, and the Tukey method was employed for multiple comparisons on trueness when equal of variance was assumed. If not, the Dunnett T3 method was used. Levene's test was used to compare the precisions between groups. The level of significance was set at 0.05.

3. Results

The intra-operator reliability was high, with an ICC of 0.985 for linear measurements and 0.997 for angular measurements. The repeatability standard deviation of the post-processing procedure was 6.8 μm/0.151°, indicating the total random errors associated with this procedure under the same testing conditions.

The Kolmogorov-Smirnov test showed that the original angular data and the transformed linear data (obtained by taking the square root of the original data) followed normal distributions. In terms of linear measurements, One-way ANOVA revealed significant differences in trueness among groups at sites 14-16 and 26-16. Similarly, significant differences in linear precision were observed at sites 22-16 and 26-16

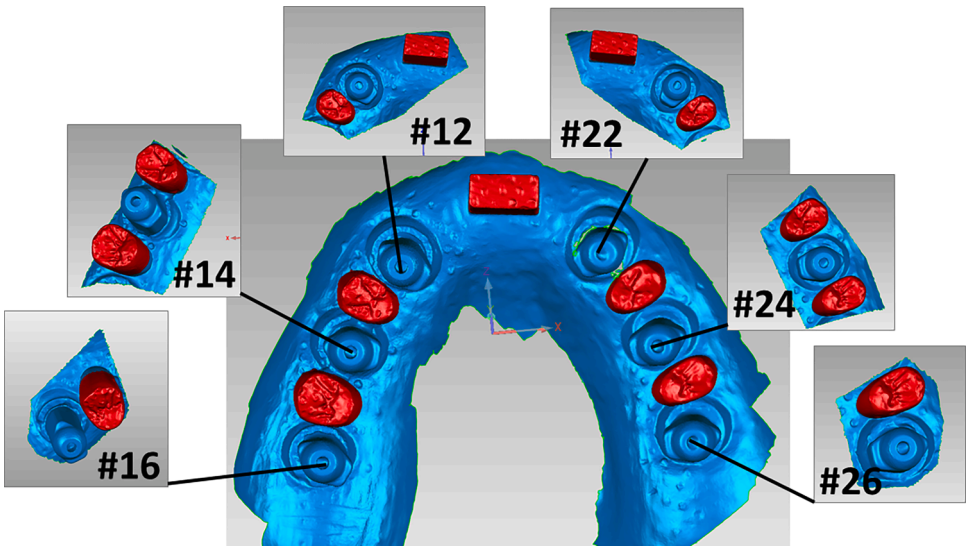

Fig. 3. Segmentation of the IOS model.

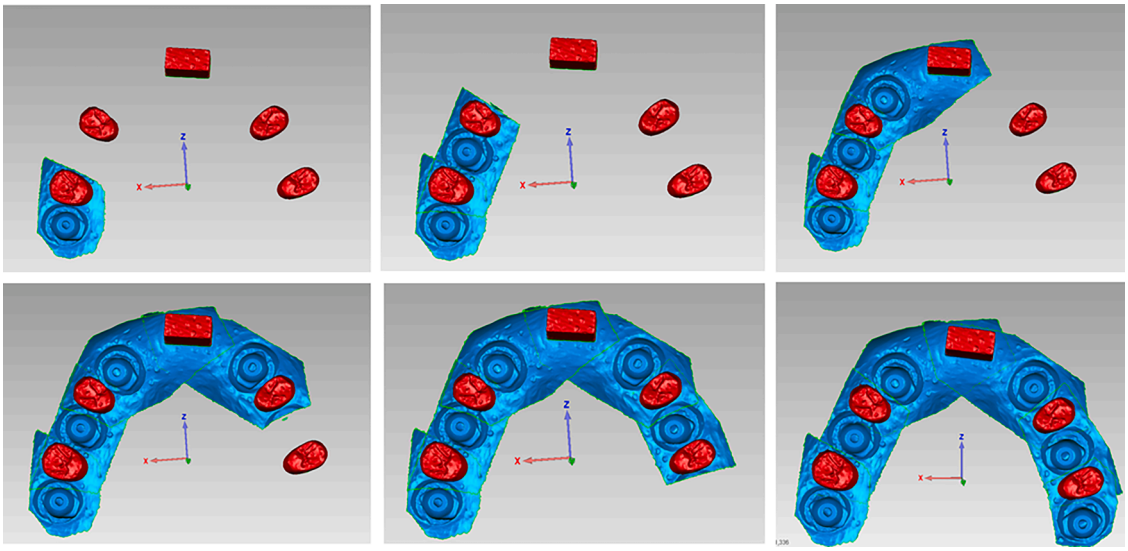

Fig. 4. Segments were aligned to the reference markers one after another.

(Fig. 7). For angular measurements, significant differences in both trueness and precision were found among groups at all sites, except for 12-16 (Fig. 8).

The data were further analyzed by pooling them into two quadrants: Q1 (16-14 and 16-12) and Q2 (16-22, 16-24, 16-26) (Table 1). Within Q1, there were no significant differences among the groups, except that the conventional group had significantly better angular trueness compared to the control and verified group ($p = 0.040$). In Q2, the verified group exhibited the best linear trueness and precision among the three groups (control trueness $p = 0.002$, precision $p < 0.001$; conventional trueness $p = 0.006$, precision $p < 0.001$). On the other hand, the conventional group showed the best angular trueness and precision (control trueness $p < 0.001$, precision $p < 0.001$; verified trueness $p < 0.001$, precision $p = 0.001$). There was no significant difference in angular trueness and precision between the control and verified group (trueness $p = 0.992$, precision $p = 0.068$).

In terms of the pooled linear outcomes, One-way ANOVA revealed a significant difference in the linear trueness among groups ($p = 0.002$). The verified group had significantly higher pooled linear trueness (29.7 μm, CI 24.8~34.6) compared to both the control group (46.6 μm, CI 37.7~55.4, $p = 0.026$) and the conventional group (51.3 μm, CI 40.9~61.7, $p = 0.003$). Levene's test also showed that the pooled linear precision of the verified group (24.8 μm) was significantly higher than that of the control group (44.7 μm, $p < 0.001$) and the conventional group (36.5 μm, $p < 0.001$), while no significant differences were observed between the control and conventional group ($p = 0.626$).

For the angular outcomes, significant differences were found among the groups in terms of angular trueness ($p < 0.001$) and precision ($p < 0.001$). The conventional group exhibited higher angular trueness (0.114°, CI 0.089~0.138) and precision (0.085°) compared to the other two groups ($p < 0.001$). However, no significant differences were found between the control and verified group in terms of angular trueness ($p = 0.986$) and precision ($p = 0.143$) (Table 1).

4. Discussion

The key finding of this *in vitro* study is that the post-processing strategy significantly improved the linear trueness and precision of IOS scans in complete-arch implant rehabilitation. However, it had no discernible impact on angular measurements. This study introduces a

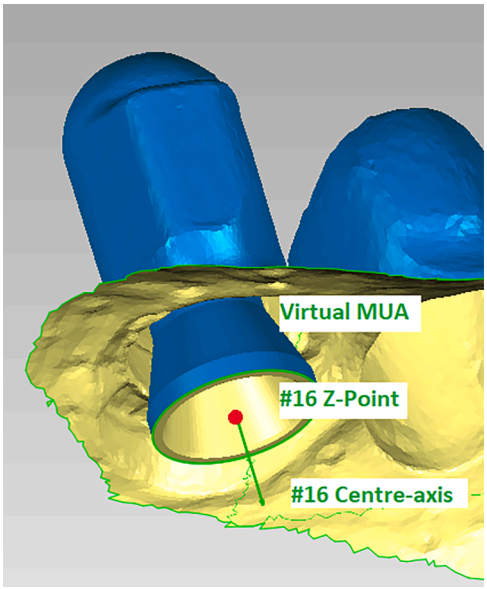

Fig. 5. Geometric features on each scan body.

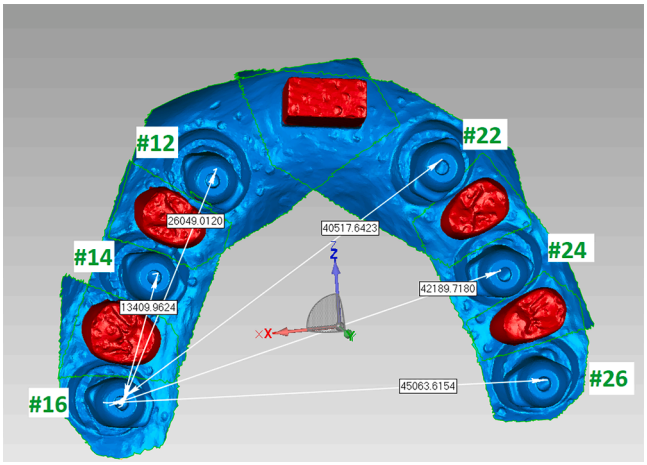

Fig. 6. Inter-Z-point distances between #16 and the other implant sites were measured.

novel approach that optimizes the implant digital workflow by incorporating CAD modification after 3D reconstruction, an area that has received limited investigation in previous studies. It is worth noting that the mean linear deviation of the virtual models decreased significantly from 46.6 ± 44.7 to 29.7 ± 24.8 μm after the post-processing procedure, particularly at the cross-arch site where it decreased from 84.0 ± 63.3 to 28.3 ± 20.2 μm. However, the mean angular deviation remained unaffected by the procedure (0.288° v.s. 0.298°). Therefore, the null hypothesis was partially rejected.

The pooled linear accuracy of the raw IO scans (46.6 ± 44.7) was comparable to that of the conventional group (51.3 ± 36.5 μm) but the error distribution pattern differed between the two techniques. The conventional group exhibited the greatest deviation in the anterior region (site 22), where there was a marked change in arch curvature. On the other hand, the raw IO scans showed the greatest deviation at the distal end of the 2nd quadrant. This suggests that while anteroposterior implant-framework misfits might occur in the conventional group, lateral misfits could be more prevalent in the IO scan group. After post-processing, the accumulated error decreased significantly, indicating that the verified model was more accurate than the conventional casts. However, the angular accuracy (0.298±0.168°) did not improve with post-processing and was greater than that of the conventional group (0.114±0.085°). This difference could be attributed to the characteristics of the impression copings and scan bodies used in the study. The impression copings in the conventional group were longer (16 mm) and rigidly splinted together, while the scan bodies and artificial landmarks in the IO scan group were shorter (11 mm) and separate. This difference in design may have made the IO scan group more susceptible to errors, resulting in higher angular deviations [7]. Therefore, it appears that the current landmarks were insufficient to eliminate angular deviations, and further optimization of the post-processing strategy is necessary in future studies.

The accumulation of errors resulting from multiple stitching poses a significant challenge for intraoral scanner (IOS) applications in complete arches [20]. Previous studies have attempted to address this issue by optimizing various factors, including view frame size, scanning speed [21], distance [22], span [23,24], ambient light [25], scanning strategy [26], and anatomic landmarks [27]. However, the improvement achieved has been shown to be limited. In this study, errors originating from the edentulous sites were eliminated by utilizing landmarks on the auxiliary device. Therefore, the remaining errors were believed to be attributed to the inherent algorithm used for image stitching of individual images. The proposed post-processing strategy aimed to reduce these errors by segmenting the implant scan bodies from the original arch and repositioning them based on reference landmarks. Since the IOS scanner demonstrated satisfactory accuracy within a single view frame [28], no compromise was made on the image quality of each scan

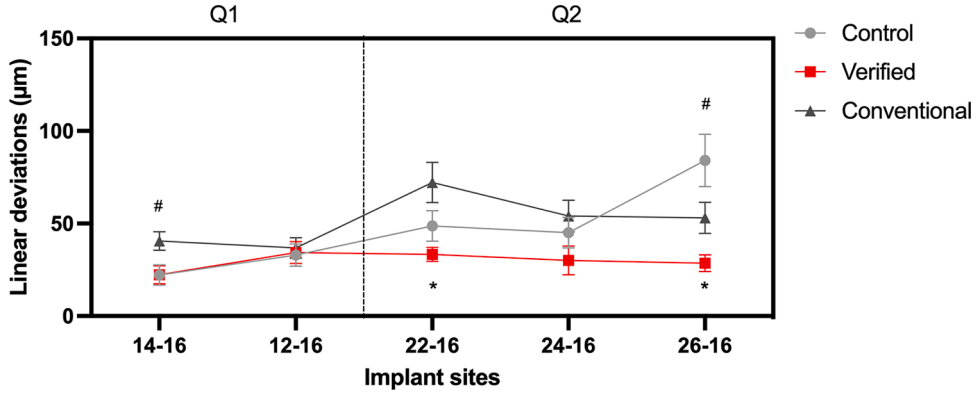

Fig. 7. The points indicated linear trueness and the error bars represented linear precision of each site. The linear trueness of the control group (gray dots) increased as the distance increased, while those of the verified group (red squares) remained stable and the conventional group (black triangles) peaked at the anterior site (22–16). *indicated a significant difference in precision; #indicated a significant difference in trueness. Q1: 1st quadrant. Q2: 2nd quadrant (For interpretation of the references to color in this figure legend, the reader is referred to the web version of this article.).

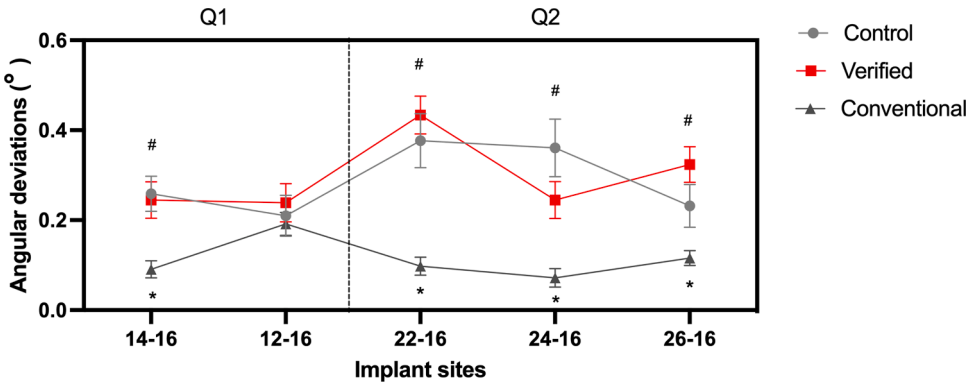

Fig. 8. The angular deviation for trueness fluctuated among the implant sites without trends. The angular deviation for trueness and precision were significantly different among groups in most implant sites. *indicated a significant difference in precision; #indicated a significant difference in trueness. Q1: 1st quadrant. Q2: 2nd quadrant.

Table 1
Linear and angular trueness and precision of the groups.

	Q1				Q2				Pooled			
	Trueness		Precision		Trueness		Precision		Trueness		Precision	
	Linear (μm)	Angular (°)	Linear (μm)	Angular (°)	Linear (μm)	Angular (°)	Linear (μm)	Angular (°)	Linear (μm)	Angular (°)	Linear (μm)	Angular (°)
Control	25.6†	0.235†	26.1†	0.158†	59.3†	0.323†	49.9†	0.221†	46.6†	0.288†	44.7†	0.202†
Verified	28.3†	0.242†	24.9†	0.154†	30.6‡	0.334†	24.9‡	0.169†	29.7‡	0.298†	24.8‡	0.168†
Conventional	38.6†	0.142‡	23.3†	0.097†	59.7†	0.095‡	41.4†	0.072‡	51.3†	0.114‡	36.5†	0.085‡

Means in column that do not share the same symbols are significantly different among groups.

body, ensuring that downstream procedures, including CAD-CAM steps, remained unaffected [29]. Additionally, there was a notable improvement in linear accuracy in the second quadrant following the implementation of the modified workflow. The mean linear deviation decreased from 64.5 ± 54.8 μm to 27.9 ± 24.1 μm. Particularly noteworthy was the remarkable 63 % reduction in linear deviation observed at the cross-arch site (#26). Although the statistical significance was not achieved for two other sites in the second quadrant (#22 and #24), they still exhibited reductions of 31 % and 46 %, respectively. These findings suggest that the modified workflow holds promising potential in reducing implant-framework misfits. However, further clinical studies will be necessary to confirm the efficacy of the proposed approach in enhancing clinical outcomes.

The present study introduced a post-processing strategy consisting of several steps, including model segmentation, landmark selection, alignment, and model merging. This procedure can be implemented using dental-specific computer-aided design (CAD) software, such as EXOCAD, which is widely accessible in dental laboratories. The entire process can typically be completed within 8 min. A significant emphasis was placed on the selection and alignment of landmarks, as these factors played a crucial role in the success of the post-processing technique [30]. To maintain precision, the same operator (Y. Pan) followed ISO-5725 guidelines and maintained an acceptable level of 6.6 μm/0.038° for the surface models' selection. In each case, 2/3 of the coronal part of the artificial landmark was selected for alignment, while the remaining 1/3 close to the resin base was excluded due to potential voids from incomplete scanning. It is worth noting that the scanner software automatically filled in the missing parts in the scan body image. However, this automated process could introduce misalignment and lead to faulty processing of the virtual scan body. Previous studies have reported errors of up to 30 μm from virtual alignment when dealing with well-scanned scan bodies [29], as well as linear discrepancies of up to 80 μm arising from improperly scanned scan bodies [31]. It has also been shown that the accuracy of different algorithms for virtual alignment of paired surface models can vary significantly [32]. These findings underscore the significance of addressing alignment errors in the CAD-CAM workflow. In this study, a two-step alignment procedure was used, which involved a coarse landmark-based pre-registration and a full-image-content based re-alignment using the ICP algorithm. This protocol is considered the most reliable as it utilizes all available information from the point clouds throughout the entire alignment process [33,34].

In the context of registration landmarks for complete-arch scanning, fiduciary spheres were deemed unsuitable due to their poor angular precision and trueness, as evidenced by previous studies [14]. The identical nature of the spheres in all directions and the absence of geometric indicators for orienting the images within the 3D coordinate system contributed to the potential rotation of matching surfaces along a random axis of the sphere. Consequently, this led to inaccurate results in the scanning process [32,35]. To address this limitation, the present study employed an auxiliary device that featured artificial teeth with distinct anatomic features, including both steep and flat surfaces. This design choice enabled quick recognition and precise matching during the registration procedure. The incorporation of anatomic features facilitated more accurate alignment of the scanned images [35,36]. However, despite the utilization of the auxiliary device, the results obtained after verification indicated that angular trueness was not significantly improved. This suggests that further advancements and developments in the design of landmarks are necessary to achieve enhanced accuracy in future studies.

The process involved in creating and utilizing the auxiliary device, as described in this study, required a considerable amount of time and manual effort. The process of creating an auxiliary device (30 min), conducting separate scans of the auxiliary device (2 min), segmenting the scans (1 min), performing separate registrations (4 min), and finally creating a single model (1 min) was labor-intensive. The process was manually conducted and required specific training and expertise. Further developments in simplifying and automating the process is needed.

In this *in vitro* study, the post-processing strategy has only been

validated at the CAD stage of the digital workflow. Therefore, further studies are needed to determine if the improved accuracy can be maintained during downstream processes. Additionally, it is important to note that the dataset was outputted and processed in the STL format, which may potentially compromise accuracy as detailed information carried by the point cloud may be lost during the format conversion to the triangular mesh. Furthermore, this study specifically examined an auxiliary device with tooth-shaped landmarks, and as such, the findings may not be applicable to other designs.

5. Conclusions

Within the limitations of this study, the following conclusions can be drawn:

(1) The proposed post-processing protocol is effective in improving the linear accuracy of IO scans for complete-arch implants, especially at the cross-arch sites.
(2) The post-processing protocol showed negligible effect on the angular accuracy.
(3) Further development in simplifying and automating the whole process is needed.

CRediT authorship contribution statement

Yu Pan: Conceptualization, Methodology, Writing – original draft, Investigation. **Xuanyi Dai:** Software, Data curation. **Fang Wan:** Methodology, Validation. **Chaoyang Song:** Validation. **James KH Tsoi:** Conceptualization, Supervision. **Edmond HN Pow:** Writing – review & editing, Supervision.

Declaration of Competing Interest

The authors declare that they have no known competing financial interests or personal relationships that could have appeared to influence the work reported in this paper.

References

[1] D. Guo, S. Mühlemann, S. Pan, Y. Zhou, R.E. Jung, A double-blind randomized within-subject study to evaluate clinical applicability of four digital workflows for the fabrication of posterior single implant crown, Clin. Oral Implants Res. (2023), https://doi.org/10.1111/clr.14171.

[2] P. Papaspyridakos, K. Vazouras, Y.w. Chen, E. Kotina, Z. Natto, K. Kang, K. Chochlidakis, Digital vs conventional implant impressions: a systematic review and meta-analysis, J. Prosthodont. 29 (8) (2020) 660–678, https://doi.org/10.1111/jopr.13211.

[3] H. Mutwalli, M. Braian, D. Mahmood, C. Larsson, Trueness and precision of three-dimensional digitizing intraoral devices, Int. J. Dent. (2018), 5189761, https://doi.org/10.1155/2018/5189761.

[4] W. Renne, M. Ludlow, J. Fryml, Z. Schurch, A. Mennito, R. Kessler, A. Lauer, Evaluation of the accuracy of 7 digital scanners: an *in vitro* analysis based on 3-dimensional comparisons, J. Prosthet. Dent. 118 (1) (2017) 36–42, https://doi.org/10.1016/j.prosdent.2016.09.024.

[5] V. Rutkunas, A. Geciauskaite, D. Jegelevicius, M. Vaitiekunas, Accuracy of digital implant impressions with intraoral scanners. A systematic review, Eur. J. Oral Implantol. 10 (Suppl 1) (2017) 101–120.

[6] D. Spagopoulos, G. Kaisarlis, F. Spagopoulou, D.J. Halazonetis, J.F. Güth, E. Papazoglou, *In vitro* trueness and precision of intraoral scanners in a four-implant complete-arch model, Dent. J. 11 (1) (2023), https://doi.org/10.3390/dj11010027.

[7] M. Revilla-León, A. Lanis, B. Yilmaz, J.C. Kois, G.O. Gallucci, Intraoral digital implant scans: parameters to improve accuracy, J. Prosthodont. (2023), https://doi.org/10.1111/jopr.13749.

[8] R. Nedelcu, P. Olsson, M. Thulin, I. Nyström, A. Thor, *In vivo* trueness and precision of full-arch implant scans using intraoral scanners with three different acquisition protocols, J. Dent. 128 (2023), 104308, https://doi.org/10.1016/j.jdent.2022.104308.

[9] S. O'Toole, P. Charalambous, A. Almatrafi, S. Mukar, S. Elsharkawy, D. Bartlett, Progress and limitations of current surface registration methods when measuring natural enamel wear, J. Dent. 112 (2021), 103738, https://doi.org/10.1016/j.jdent.2021.103738.

[10] T. Fluegge, W. Att, M. Metzger, K. Nelson, A novel method to evaluate precision of optical implant impressions with commercial scan bodies—an experimental approach, J. Prosthodont. 26 (1) (2017) 34–41, https://doi.org/10.1111/jopr.12362.

[11] Y. Pan, J.M.Y. Tam, J.K.H. Tsoi, W.Y.H. Lam, E.H.N. Pow, Reproducibility of laboratory scanning of multiple implants in complete edentulous arch: effect of scan bodies, J. Dent. 96 (2020), 103329, https://doi.org/10.1016/j.jdent.2020.103329.

[12] A. Schmidt, J.W. Billig, M.A. Schlenz, P. Rehmann, B. Wostmann, Influence of the accuracy of intraoral scanbodies on implant position: differences in manufacturing tolerances, Int. J. Prosthodont. 32 (5) (2019) 430–432, https://doi.org/10.11607/ijp.6371.

[13] M. Iturrate, H. Eguiraun, O. Etxaniz, E. Solaberrieta, Accuracy analysis of complete-arch digital scans in edentulous arches when using an auxiliary geometric device, J. Prosthet. Dent. 121 (3) (2019) 447–454, https://doi.org/10.1016/j.prosdent.2018.09.017.

[14] Y. Pan, J.K. Tsoi, W.Y.H. Lam, K. Zhao, E.H.N. Pow, Improving intraoral implant scanning with a novel auxiliary device: an *in-vitro* study, Clin. Oral Implants Res. 30 (12) (2021) 1466–1473, https://doi.org/10.1111/clr.13847.

[15] E. Roig, M. Roig, L.C. Garza, S. Costa, P. Maia, J. Espona, Fit of complete-arch implant-supported prostheses produced from an intraoral scan by using an auxiliary device and from an elastomeric impression: a pilot clinical trial, J. Prosthet. Dent. 128 (3) (2022) 404–414, https://doi.org/10.1016/j.prosdent.2020.10.024.

[16] H. Rudolph, S. Quaas, R.G. Luthardt, Matching point clouds: limits and possibilities, Int. J. Comput. Dent. 5 (2–3) (2002) 155–164.

[17] L. Tapie, N. Lebon, B. Mawussi, H. Fron Chabouis, F. Duret, J.P. Attal, Understanding dental CAD/CAM for restorations–the digital workflow from a mechanical engineering viewpoint, Int. J. Comput. Dent. 18 (1) (2015) 21–44.

[18] L. Tapie, N. Lebon, B. Mawussi, H. Fron-Chabouis, F. Duret, J.-P. Attal, Understanding dental CAD/CAM for restorations–accuracy from a mechanical engineering viewpoint, Int. J. Comput. Dent. 18 (4) (2015) 343–367.

[19] B. Gimenez, G. Pradies, F. Martinez-Rus, M. Ozcan, Accuracy of two digital implant impression systems based on confocal microscopy with variations in customized software and clinical parameters, Int. J. Oral Maxillofac. Implants 30 (1) (2015) 56–64, https://doi.org/10.11607/jomi.3689.

[20] R. Natsubori, S. Fukazawa, T. Chiba, N. Tanabe, H. Kihara, H. Kondo, *In vitro* comparative analysis of scanning accuracy of intraoral and laboratory scanners in measuring the distance between multiple implants, Int. J. Implant Dent. 8 (1) (2022) 18, https://doi.org/10.1186/s40729-022-00416-4.

[21] H. An, E.E. Langas, A.S. Gill, Effect of scanning speed, scanning pattern, and tip size on the accuracy of intraoral digital scans, J. Prosthet. Dent. (2022), https://doi.org/10.1016/j.prosdent.2022.05.005.

[22] R.N. Rotar, A.B. Faur, D. Pop, A. Jivanescu, Scanning distance influence on the intraoral scanning accuracy-an *in vitro* study, Materials 15 (9) (2022) 3061, https://doi.org/10.3390/ma15093061.

[23] M. Gómez-Polo, R. Ortega, A. Sallorenzo, R. Agustín-Panadero, A.B. Barmak, J. C. Kois, M. Revilla-León, Influence of the surface humidity, implant angulation, and interimplant distance on the accuracy and scanning time of complete-arch implant scans, J. Dent. 127 (2022), 104307, https://doi.org/10.1016/j.jdent.2022.104307.

[24] Y. Chen, Z. Zhai, S. Watanabe, T. Nakano, S. Ishigaki, Understanding the effect of scan spans on the accuracy of intraoral and desktop scanners, J. Dent. 124 (2022), 104220, https://doi.org/10.1016/j.jdent.2022.104220.

[25] M. Revilla-León, A. Gohil, A.B. Barmak, M. Gómez-Polo, J.A. Pérez-Barquero, W. Att, J.C. Kois, Influence of ambient temperature changes on intraoral scanning accuracy, J. Prosthet. Dent. (2022), https://doi.org/10.1016/j.prosdent.2022.01.012.

[26] S. Pattamavilai, C. Ongthiemsak, Accuracy of intraoral scanners in different complete arch scan patterns, J. Prosthet. Dent. (2022), https://doi.org/10.1016/j.prosdent.2021.12.026.

[27] P. Kanjanasavitree, P. Thammajaruk, M. Guazzato, Comparison of different artificial landmarks and scanning patterns on the complete-arch implant intraoral digital scans, J. Dent. 125 (2022), 104266, https://doi.org/10.1016/j.jdent.2022.104266.

[28] M. Zimmermann, A. Ender, A. Mehl, Local accuracy of actual intraoral scanning systems for single-tooth preparations *in vitro*, J. Am. Dent. Assoc. 151 (2) (2020) 127–135, https://doi.org/10.1016/j.adaj.2019.10.022.

[29] Y. Pan, J.K.H. Tsoi, W.Y.H. Lam, Z. Chen, E.H.N. Pow, Does the geometry of scan bodies affect the alignment accuracy of computer-aided design in implant digital workflow: an *in vitro* study? Clin. Oral Implants Res. 33 (3) (2021) 313–321, https://doi.org/10.1111/clr.13890.

[30] J.H. Park, G.H. Lee, D.N. Moon, K.D. Yun, J.C. Kim, K.C. Lee, Creation of digital virtual patient by integrating CBCT, intraoral scan, 3D facial scan: an approach to methodology for integration accuracy, J. Craniofac. Surg. 33 (4) (2022) e396–e398, https://doi.org/10.1097/scs.0000000000008275.

[31] S.-W. Park, Y.-D. Choi, D.-H. Lee, The effect of the improperly scanned scan body images on the accuracy of virtual implant positioning in computer-aided design software, J. Adv. Prosthodont. 12 (3) (2020) 107–113.

[32] J.B.A. Maintz, M.A. Viergever, A survey of medical image registration, Med. Image Anal. 2 (1) (1998) 1–36, https://doi.org/10.1016/S1361-8415(01)80026-8.

[33] S. Park, H.C. Kang, J. Lee, J. Shin, Y.G. Shin, An enhanced method for registration of dental surfaces partially scanned by a 3D dental laser scanning, Comput. Methods Programs Biomed. 118 (1) (2015) 11–22, https://doi.org/10.1016/j.cmpb.2014.09.007.

[34] S.J. Lee, M.K. Park, K.H. Lee, Full 3D surface reconstruction of partial scan data with noise and different levels of scale, J. Mech. Sci. Technol. 28 (8) (2014) 3171–3180, https://doi.org/10.1007/s12206-014-0726-x.
[35] R. Szeliski, Image Alignment and Stitching, in: R. Szeliski (Ed.), Computer Vision: Algorithms and Applications, Springer International Publishing, Cham, 2022, pp. 401–441.
[36] R.J. Campbell, P.J. Flynn, A survey of free-form object representation and recognition techniques, Comput. Vis. Image Underst. 81 (2) (2001) 166–210, https://doi.org/10.1006/cviu.2000.0889.